Structural Engineering and Mechanics, *Vol. 49, No. 5 (2014) 569-595*
DOI: http://dx.doi.org/10.12989/sem.2014.49.5.569

Post-buckling finite strip analysis of thick functionally graded plates

M. Hajikazemi*[1], H.R. Ovesy[1a], H. Assaee[2b] and M.H. Sadr[1c]

[1]*Aerospace Engineering Department and Center of Excellence in Computational Aerospace Engineering, Amirkabir University of Technology, Tehran, Iran*
[2]*Mechanical & Aerospace Engineering Department, Shiraz University of Technology, Shiraz, Iran*

(Received September 26, 2013, Revised December 28, 2013, Accepted January 12, 2014)

Abstract. In this paper, a novel semi-energy finite strip method (FSM) is developed based on the concept of first order shear deformation theory (FSDT) in order to attempt the post-buckling solution for thin and relatively thick functionally graded (FG) plates under uniform end-shortening. In order to study the effects of through-the-thickness shear stresses on the post-buckling behavior of FG plates, two previously developed finite strip methods, i.e., semi-energy FSM based on the concept of classical laminated plate theory (CLPT) and a CLPT full-energy FSM, are also implemented. Moreover, the effects of aspect ratio on initial post-buckling stiffness of FG rectangular plates are studied. It has been shown that the variation of the ratio of initial post-buckling stiffness to pre-buckling stiffness (S^*/S) with respect to aspects ratios is quite independent of volume fractions of constituents in thin FG plates. It has also been seen that the universal curve representing the variation of (S^*/S) with aspect ratio of a FG plate demonstrate a saw shape curve. Moreover, it is revealed that for the thin FG plates in contrast to relatively thick plates, the variations of non-dimensional load versus end-shortening is independent of ceramic-metal volume fraction index. This means that the post-buckling behavior of thin FG plates and the thin pure isotropic plates is similar. The results are discussed in detail and compared with those obtained from finite element method (FEM) of analysis. The study of the results may have a great influence in design of FG plates encountering post-buckling behavior.

Keywords: post-buckling; FG material; finite strip; semi-energy; first order shear deformation theory

1. Introduction

Functionally graded materials (FGMs) are new classes of heterogeneous materials that are mainly used to improve the structural efficiency in many engineering applications (Suresh and Mortensen 1998). Originally, the researches on the FGMs began in 1984 by the material scientists to produce thermal barrier materials (Koizumi 1997). FGMs are usually made from a mixture of metals and ceramics. By gradually varying the volume fraction of constituent materials, the material properties of FGMs exhibit a smooth and continuous change from one surface to another,

*Corresponding author, Ph.D. Student, E-mail: hajikazemi@aut.ac.ir
[a]Professor, E-mail: ovesy@aut.ac.ir
[b]Assistant Professor, E-mail: assaee@sutech.ac.ir
[c]Associate Professor, E-mail: sadr@aut.ac.ir

http://www.techno-press.org/?journal=sem&subpage=8 ISSN: 1225-4568 (Print), 1598-6217 (Online)

thus eliminating interface problems. As a result, FGM has extended its applications in aerospace, mechanical, marine and structural engineering due to its advantages compared to the classically used laminated composites. With escalating application of functionally graded materials, the attention has been drawn to the investigation of the non-linear behavior of the structures made up of these materials. In order to get the reader acquainted with some of the past works, a brief review is provided. The transient nonlinear thermo-elastic behavior of a functionally graded ceramic/ metal plate is investigated by Praveen and Reddy (1998) applying the Von-Kármán plate theory and the finite element method. Reddy (2000) has investigated the geometrically nonlinear behavior of FGM plates subjected to transverse loads and provided several illustrative examples comparing the classical plate theory (CPT) to the first- and third-order shear deformation plate theories (SDPT). Woo and Meguid (2001) have given an analytical solution for large deflection of FGM plates and shallow shells. In their studies, the considered thermal load arises from the one-dimensional steady heat conduction in the plate thickness direction, but the material properties are temperature independent. Yang and Shen (2003) have investigated the large deflection and post-buckling responses of FG rectangular plates under transverse and in-plane loads by using a semi-analytical approach. In their analysis, a perturbation technique in conjunction with one-dimensional differential quadrature approximation and Galerkin procedure were employed. GhannadPour and Alinia (2006) have given an analytical solution for large deflection behavior of thin functionally graded plates under pressure load using CPT. Anandrao *et al*. (2010) have investigated the thermal post-buckling behavior of uniform slender FGM beams using the classical Rayleigh-Ritz formulation and the finite element method. Sadr *et al*. (2011) have studied the large deflection behavior of thick FG plates based on the third-order SDPT. In their studies, the material properties of the functionally graded plate are assumed to vary continuously through the thickness of the plate, according to the simple power law distribution in terms of the volume fractions of constituents and the solution was obtained using the multi term series approximation. Anandrao *et al*. (2012) have also studied the large amplitude free vibration and thermal post-buckling of shear flexible FG beams using finite element formulation based on first order Timoshenko beam theory. Kocaturk and Akbas (2012) have analyzed the post-buckling of functionally graded Timoshenko beam subjected to thermal loading by using the total Lagrangian Timoshenko beam element approximation. They also assumed that the material properties of the beam change in the thickness direction according to a power-law function.

The post-buckling behavior of a plate can be analyzed by solving the Von-Kármán non-linear equations (Von-Karman 1910), together with the appropriate boundary conditions. Unfortunately, the Von-Kármán equations are coupled and forth-order and thus no rigorous solutions are available. This has prepared a ground for development of the approximate methods such as finite element method, finite strip method (FSM), etc.

The finite strip method is one version of finite element method that is well suited to the accurate and efficient analysis of both single rectangular plates and complicated prismatic plate structures (Cheung 1976). Early works were concerned with the use of FSM in predicting the geometrically non-linear response of single rectangular plates while prismatic plate structures are those of Sridharan and Graves-Smith (1981), and Hancock (1981). In the field of linear buckling and vibration analysis, the method has been developed by Dawe (2002) for the analysis of complicated plate structures formed of composite laminated material having very general material properties. Recently, Kasaeian *et al*. (2011) have used the finite strip method in order to study the inelastic local buckling of curved isotropic plates. More recently, Cuong (2013) has used 3-nodal line semi-analytical Mindlin-Reissner finite strip in the buckling analysis of thin-walled members,

which are subjected to arbitrary loads. Moreover, Pham and Hancock (2013) have studied the shear buckling of channels using the semi-analytical and spline finite strip methods. In addition, Ovesy and his co-workers have made several contributions by developing two variants of finite strip methods, namely the full-energy (Ovesy *et al*. 2006, Ovesy and Ghannadpour 2007, Sherafat *et al*. 2013) and semi-energy (Assaee and Ovesy 2007, 2008, Ovesy and Ghannadpour 2009, Ovesy and Assaee 2009, Ovesy *et al*. 2011, 2012, Assaee *et al*. 2012) finite strip approaches. These methods were applied to the analyses of the geometrically non-linear response of rectangular composite laminated plates with various lay-ups, loading and boundary conditions.

The concept of second FSM variant, which was originally developed by authors of current paper, is based on semi-energy method as referred to by Rhodes and Harvey (1977). The semi-energy method was first used by Marguerre (1937), and has since been used by various researchers. One of the main advantages of the semi-energy FSM is the fact that the semi-energy FSM is based on the closed form solution of Von-Kármán's compatibility equation in order to derive analytical shape functions for in-plane displacement fields. This can be considered as the major difference between the semi-energy formulations and those based on the full-energy assumptions where the in-plane and out-plane displacements as well as the rotations are all postulated by the appropriate deflected forms in latter FSM. In the developed version of the semi-energy finite strip approach (Assaee and Ovesy 2007, 2008, Ovesy and Ghannadpour 2009, Ovesy and Assaee 2009, Assaee *et al*. 2012), which is suitable for the post-buckling analysis of thin composite plate structures, the out-of-plane displacement field of the finite strip is the only displacement which is postulated by a deflected form due to the application of classic laminated plate theory (CLPT). More recently, Ovesy and his co-workers have enhanced the formulation of the previously developed CLPT semi-energy finite strip approach in order to investigate through-the-thickness shearing effects for symmetric (Ovesy *et al*. 2011) and anti-symmetric angle-ply (Ovesy *et al*. 2012) laminate configurations under simply-supported boundary conditions at loaded ends by implementing the first order shear deformation theory (FSDT). Thus, in addition to the out-of-plane displacement field of the finite strip, the rotations with respect to x and y axes are also postulated by two deflected forms. It is noted that for symmetric lay-ups, the effects of postulated rotations have not appeared in the corresponding Von-Kármán's compatibility equation and the subsequent in-plane displacements. Moreover, for anti-symmetric angle-ply laminates, these effects have appeared only through B_{13} and B_{23} terms of coupling stiffness matrix. It is realized that the difference between CLPT and FSDT semi-energy results has become noticeable as the thickness increases.

In the current work, as distinct from the latter publications by the same authors (Ovesy *et al*. 2011, 2012), the plate is assumed to be made from FGM and also under clamped boundary conditions at loaded ends. Thus, due to the bending-stretching coupling effects, the two postulated rotations have appeared in the corresponding Von-Kármán's compatibility equation through the additional coupling terms (B_{11}, B_{12}, B_{22}, B_{33}) beside the assumed out-of-plane displacement. Having solved the Von-Kármán's compatibility equation exactly, the corresponding forms of the in-plane stresses and displacements are obtained. The resulted in-plane displacements, in which the effects of independently assumed rotations have clearly been taken into account for FG plates, are therefore more sophisticated than those obtained in the earlier publications for symmetric and anti-symmetric angle-ply laminates under simply supported boundary conditions at loaded ends. The solution of Von-Kármán's compatibility equation and the postulated deflected forms are then used to evaluate the potential energy of the respective finite strip. Finally, by invoking the Principle of Minimum Potential Energy, the unknown deflection coefficients are determined and

thus the problem is solved. Moreover, in order to investigate the effects of through-the-thickness shear stresses on the post-buckling behavior of FG plates, two finite strip methods based on the concept of classic laminated plate theory with full-energy and semi-energy assumptions are also employed. It is also noted that the solution of Von-Karman's compatibility equation related to a thin FG clamped finite strip based on the concept of CLPT was first attempted in the conference papers (Ovesy *et al*. 2009, Assaee *et al*. 2010). In this paper the theoretical formulations of the previously developed CLPT FSM are also presented in further detail. The post-buckling behavior of thin and relatively thick rectangular FG plates with clamped out-of-plane boundary conditions at its loaded ends and simply-supported boundary conditions at unloaded edges is analyzed. In order to validate the FSM results, they are compared with those obtained from finite element method (FEM) of analysis. The FEM analysis has been carried out using general purpose ANSYS software. It has been shown that for a given level of accuracy in the results, the developed semi-energy FSMs requires markedly lower number of degrees of freedom compared to that needed by full-energy FSM and FEM. Hence, the semi-energy FSM is more computationally efficient than the conventional energy based schemes. In addition, the effects of aspect ratio on buckling and initial post-buckling behavior of thin FG plates are studied. The analysis of results has revealed that the ratio of initial post-buckling stiffness to pre-buckling stiffness (i.e., S^*/S), for the thin FG plates analyzed in this paper, is only dependent on the aspect ratio of plates and independent of ceramic-metal volume fraction index. Moreover, the variations of S^*/S with reference to FG aspect ratio for mentioned plates demonstrate a *saw shape* curve, which is highly influenced by buckling mode shape of FG plate. In addition, it has been shown that for the thin FG plates, the variations of non-dimensional load versus end-shortening is independent of ceramic-metal volume fraction index. It is also revealed that the post-buckling behavior of thin FG plates and the thin pure isotropic plates are equal.

2. Theoretical formulations

A FG rectangular plate of length *L*, width *b* and thickness *h*, made from a mixture of ceramics and metals is considered. The composition is assumed to be varied in such a way that the top surface of the plate (*z=h/2*) is ceramic-rich, whereas the bottom surface (*z=-h/2)* is metal-rich. Thus, the material properties of the FG plate, such as the Young's modulus (*E*) and the shear modulus (*G*) are functions of depth (*z*). These functions are desired to be continuous, simple and capable of exhibiting curvature, both "concave upward" and "concave downward" (Markworth *et al*. 1995). In this study the simple power law, which has all the desired properties, is used. The function $\vartheta(z)$, which denotes a typical material property (*E*, *G*), is given as

$$\vartheta(z) = \vartheta_{tb}\left(\frac{z}{h}+\frac{1}{2}\right)^n + \vartheta_b \qquad \textit{Where} \qquad \vartheta_{tb} = \vartheta_t - \vartheta_b \tag{1}$$

where $\vartheta_t(z)$ and $\vartheta_b(z)$ denote values of the variables at top and bottom surfaces of plates, respectively. The parameter *n*, which is known as the volume fraction index and is a non-negative real number, indicates the material variation profile through the thickness direction. Whilst *n=0* corresponds to pure ceramic, the value of *n* can reach infinity, in the limit and in theory of course, corresponding to the pure metal plate. With the above assumptions, the plate stiffness coefficients are defined (Sadr *et al*. 2011, Shen 2009). In subsequent sections of the paper the fundamental

elements of the buckling and post-buckling analyses of rectangular FG plates are discussed in detail.

3. Buckling analysis of FG rectangular plates using Rayleigh-Ritz approach based on CLPT assumptions

For a rectangular FG plate of length L and width b a Right-Handed Cartesian Coordinate System is assumed. The x-axis lies parallel to the longitudinal edge and hence the y-axis is perpendicular to x-axis and parallel to transverse edge of rectangular plate. Moreover, z-axis is assumed to be normal to plate. u, υ and w are displacement functions in x, y and z directions, respectively. The plate is assumed to be uniformly loaded in x-direction and σ_x denotes the axial stress. The rectangular plates are assumed to be clamped out-of-plane at loaded ends (i.e., x=0, L) and hinged at the unloaded edges (i.e., y=*0, b*).

It is noted that as the FGM may exhibit a coupling between in-plane loads and out-of-plane moments and twisting curvatures, it may be expected that abovementioned FG plate encounters out-of-plane deformations from the onset of loading and hence the buckling may not occur. However, with regard to justification proposed by Leissa (1986) for the cases under study in this paper, as the loaded edges of FG plate are clamped out-of-plane, it will remain flat up to the buckling load and hence, a bifurcation point will be occurred.

To evaluate buckling load capacity of mentioned FG plates the Rayleigh-Ritz approach is considered. In this method which is based on minimization of total potential energy of FG plate due to the perturbations imposed to FG plate a series of buckling displacement functions should be defined. The following trigonometric displacement functions that satisfy the essential boundary conditions are found to be suitable for the buckling analysis (Allen and Bulson 1980).

$$\begin{aligned} u &= \sum_{i=1}^{4} \alpha_i \sin\left(\frac{\pi y}{b}\right)\cos\left(\frac{i\pi x}{L}\right) \\ \upsilon &= \sum_{i=1}^{4} \beta_i \cos\left(\frac{\pi y}{b}\right)\sin\left(\frac{i\pi x}{L}\right) \\ w &= \sum_{i=1}^{3} \lambda_i \sin\left(\frac{\pi y}{b}\right)\sin\left(\frac{\pi x}{L}\right)\sin\left(\frac{i\pi x}{L}\right) \end{aligned} \tag{2}$$

Where α_i, β_i and λ_i are the buckling displacement unknown coefficients. The linear middle surface strains in terms of plate displacements u and υ as well as linear bending and twisting curvatures of the middle surface in terms of w, which cause additional linear strains at positions away from the middle surface through the FG plate thickness based on CLPT assumptions, are given in Eq. (3).

$$\left[\varepsilon_L\right]^T = \left\{\frac{\partial u}{\partial x}, \frac{\partial \upsilon}{\partial y}, \frac{\partial u}{\partial y} + \frac{\partial \upsilon}{\partial x}\right\} \qquad \left[\phi\right]^T = \left\{-\frac{\partial^2 w}{\partial x^2}, -\frac{\partial^2 w}{\partial y^2}, -2\frac{\partial^2 w}{\partial x \partial y}\right\} \tag{3}$$

The total potential energy of FG plate is presented as following equation

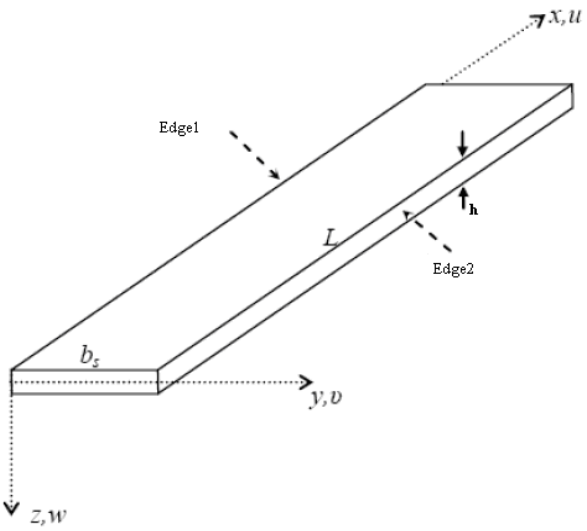

Fig. 1 FG finite strip and related coordinates

$$U = \frac{1}{2}\int_0^L \int_0^b \{[\varepsilon_L]^T [A][\varepsilon_L] + 2[\varepsilon_L]^T [B][\phi] + [\phi]^T [D][\phi]\}\, dx\, dy$$
$$+ \frac{h}{2}\sigma_x \int_0^L \int_0^b ((\frac{\partial u}{\partial x})^2 + (\frac{\partial \upsilon}{\partial x})^2 + (\frac{\partial w}{\partial x})^2)\, dx\, dy \tag{4}$$

The matrices [A], [B] and [D] are the usual in-plane, coupling and flexural stiffness matrices of FG materials, respectively. By substituting u, υ and w in Eq. (3) and then substituting the resultant linear strains, bending and twisting curvatures in Eq. (4) and carrying out the integration, the strain energy in terms of the displacement unknown coefficients is derived. By invoking the principle of minimum potential energy, a set of linear algebraic equations will be obtained which corresponds to an eigen-value problem. The evaluated eigen-values are in fact the buckling load coefficients and the minimum eigen-value represents the critical buckling load capacity of the FG plate.

4. Semi-energy finite strip formulation using FSDT

The semi-energy post-buckling theory has been developed for an initially flat FG finite strip shown in Fig. 1. The FG strip is clamped out-of-plane at both ends (i.e., at end x=0 and L), and is subjected to a uniform end shortening $\bar{u}$ at end x=L only. The degrees of freedom (DOF) are depicted in Fig. 2 for a finite strip with FSDT assumptions. It may be noted that u, v, w, φ_x & φ_y correspond to the mid-plane displacements and rotations. The degrees of freedom are defined at each nodal line and inside the strip. The boundary conditions at loaded ends of the finite strip are summarized as follows

$$w = \varphi_x = N_{xy} = 0 \qquad at\ x = 0\ \&\ L \qquad and \qquad u = \begin{cases} 0 & at\ x = 0 \\ -\bar{u} & at\ x = L \end{cases} \tag{5}$$

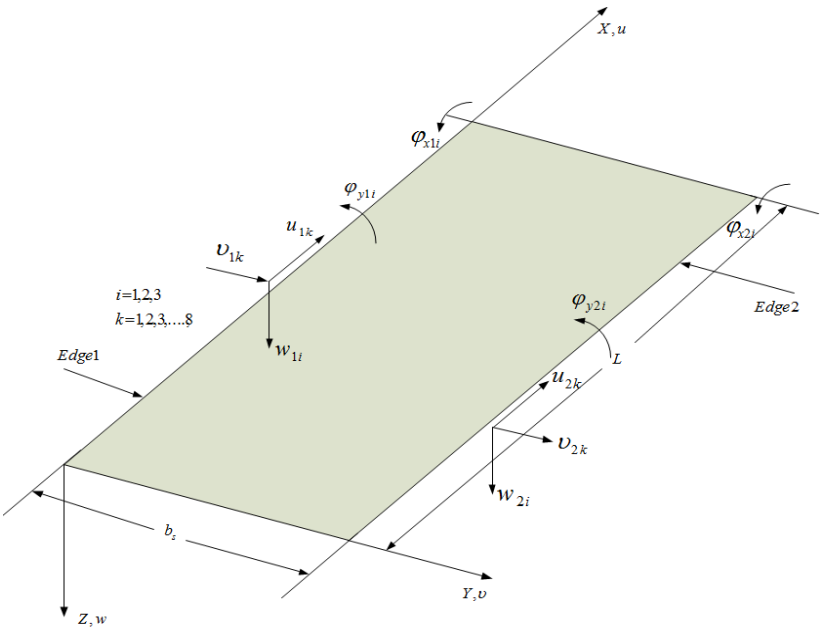

Fig. 2 Degrees of freedom for the FG finite strip with FSDT assumptions

The Von Karman's compatibility equation for large deflections of arbitrary lay-up laminated plates as given in Ref. (Chai 1989) is modified for FG plates as Eq. (6) in which the FSDT assumptions are incorporated

$$\nabla^4 F = A_{22}^* \frac{\partial^4 F}{\partial x^4} + (2A_{12}^* + A_{33}^*) \frac{\partial^4 F}{\partial x^2 \partial y^2} + A_{11}^* \frac{\partial^4 F}{\partial y^4} = \left(\frac{\partial^2 w}{\partial x \partial y} \right)^2 - \left(\frac{\partial^2 w}{\partial x^2} \right) \left(\frac{\partial^2 w}{\partial y^2} \right) - B_{21}^* \left(\frac{\partial^3 \varphi_x}{\partial x^3} \right)$$
$$- B_{12}^* \left(\frac{\partial^3 \varphi_y}{\partial y^3} \right) + (B_{33}^* - B_{22}^*) \left(\frac{\partial^3 \varphi_y}{\partial x^2 \partial y} \right) + (B_{33}^* - B_{11}^*) \left(\frac{\partial^3 \varphi_x}{\partial y^2 \partial x} \right), \tag{6}$$

Where A^* is the inverse of in-plane stiffness matrix of the FG plate (i.e., $A^*=A^{-1}$) and B^* is evaluated as $B^*=-A^*B$ where B is coupling between in-plane and out-of-plane stiffness matrix, the function F (i.e., $F=F(x,y)$) is the so called Airy stress functions which are defined as follows

$$N_x = \sigma_{xx} \cdot h = \frac{\partial^2 F}{\partial y^2}, \quad N_y = \sigma_{yy} \cdot h = \frac{\partial^2 F}{\partial x^2}, \quad N_{xy} = \sigma_{xy} \cdot h = -\frac{\partial^2 F}{\partial x \partial y}$$
$$\tau_{xz} = \frac{Q_x}{h}, \quad \tau_{yz} = \frac{Q_y}{h} \tag{7}$$

Where N_x, N_y are the in-plane axial forces per width, N_{xy} is the shear forces per width, Q_x, Q_y are shear stress resultant through-the-thickness and σ_{xx}, σ_{yy}, σ_{xy}, τ_{xz}, τ_{yz} are the corresponding average stresses. The following functions are found to be suitable to represent the out-of-plane displacement and rotations fields with respect to x, y coordinates.

$$w = \sum_{i=1}^{N} f_i(y)\sin(i\zeta x)\sin(\zeta x)$$

$$\varphi_x = \sum_{i=1}^{N} g_i(y)\cos(i\zeta x)\sin(\zeta x)$$

$$\varphi_y = \sum_{i=1}^{N} s_i(y)\sin(i\zeta x)\sin(\zeta x) \quad , \qquad \zeta = \frac{\pi}{L}$$

$$f_i(y) = (1-\frac{19}{3}\eta+\frac{32}{3}\eta^2-\frac{16}{3}\eta^3)w_{1i} + (8\eta-\frac{56}{3}\eta^2+\frac{32}{3}\eta^3)w_{1\frac{1}{4}i} +$$

$$(-\frac{8}{3}\eta+\frac{40}{3}\eta^2-\frac{32}{3}\eta^3)w_{1\frac{3}{4}i} + (\eta-\frac{16}{3}\eta^2+\frac{16}{3}\eta^3)w_{2i}$$

$$g_i(y) = (1+2\eta^2-3\eta)\varphi_{x_{1i}} + (-4\eta^2+4\eta)\varphi_{x_{1\frac{1}{2}i}} + (2\eta^2-\eta)\varphi_{x_{2i}}$$

$$s_i(y) = (1+2\eta^2-3\eta)\varphi_{y_{1i}} + (-4\eta^2+4\eta)\varphi_{y_{1\frac{1}{2}i}} + (2\eta^2-\eta)\varphi_{y_{2i}}, \qquad \eta = \frac{y}{b_s} \tag{8}$$

In the above expression $w_{1i}, w_{1\frac{1}{4}i}, w_{1\frac{3}{4}i}, w_{2i}, \varphi_{x_{1i}}, \varphi_{x_{1\frac{1}{2}i}}, \varphi_{x_{2i}}, \varphi_{y_{1i}}, \varphi_{y_{1\frac{1}{2}i}}, \varphi_{y_{2i}}$ (where i=1…N) are the undetermined displacement parameters of the strip. The first subscript of the displacement parameters refers to interpolated values of the corresponding parameter at edge 1 (e.g., w_{1i}), at $b_s/4$ distance away from edge 1 (e.g., $w_{1\frac{1}{4}i}$), at midway between two edges (e.g., $\varphi_{x_{1\frac{1}{2}i}}$), at $3b_s/4$ distance away from edge 1 (e.g., $w_{1\frac{3}{4}i}$), or finally at edge 2 (e.g., w_{2i}). The second subscript (i.e., i) refers to the corresponding harmonic terms. It is noted that the investigation on the sensitivity of the semi-energy FSM analysis to the number of harmonic terms in the postulated series has revealed that the early stages of the post-buckling behaviour of FG plates can be predicted with a very good accuracy by using three first harmonic terms (i.e., N=3in Eq. (8)).

The displacement fields are then substituted into Eq. (6) in order to find the corresponding in-plane displacement functions. In this process, the stress function F may be considered as follows

$$\begin{aligned} F(x,y) = {} & F_0(y) + F_1(y)\cos(\zeta x) + F_2(y)\cos(2\zeta x) + F_3(y)\cos(3\zeta x) + F_4(y)\cos(4\zeta x) \\ & + F_5(y)\cos(5\zeta x) + F_6(y)\cos(6\zeta x) + F_7(y)\cos(7\zeta x) + F_8(y)\cos(8\zeta x) \end{aligned} \tag{9}$$

Substituting F from Eq. (9) and w, φ_x, φ_y from Eq. (8) into Eq. (6), a set of forth-order ordinary differential equations will be achieved as Eq. (10).

$$\begin{cases} A_{11}^* F_0^{''''} = \zeta^2 \Psi_0(f_i, g_i, s_i) \\ A_{11}^* F_k^{''''} - (k\zeta)^2(2A_{12}^* + A_{33}^*)F_k^{''} + (k\zeta)^4 A_{22}^* F_k = \zeta^2 \Psi_k(f_i, g_i, s_i) \end{cases} \tag{10}$$

$$\text{where } k = 1,2,...,8 \quad \text{and} \quad i = 1,2,3$$

It is noted that the prime sign designates the derivatives of the corresponding parameter with respect to *y*, thus, for example $F_0''' = \partial^4 F_0 / \partial y^4$. It is also noted that Ψ_0, Ψ_1, Ψ_2 … Ψ_8 are known functions and can be derived analytically. The first equation can be solved easily, but the solutions for the remaining eight equations are composed of two parts, namely the particular integral solutions and the complementary function solutions. The particular integral solutions depend on the functions $f_i(y)$, $g_i(y)$, $s_i(y)$ (where i=1,2,3) only, thus it can be conveniently evaluated. But, for the complementary function solutions three cases may appear in accordance with the sign of DELTA of the forth-order characteristic equation of the differential equations, which is given as

$$\Delta = \left(2A_{12}^* + A_{33}^*\right)^2 - 4A_{11}^* A_{22}^* \tag{11}$$

Based on the sign of DELTA the following solutions can be considered for the mentioned stress function (see Eq. (9)).

If $\Delta > 0$ Then

$$F_k(y) = C_{k1}\cosh(My) + C_{k2}\sinh(My) + C_{k3}\cosh(Ny) + C_{k4}\sinh(Ny) + \Phi_k(y)$$

where

$$M = \sqrt{\frac{2A_{12}^* + A_{33}^* + \sqrt{\Delta}}{2A_{11}^*}}(k\zeta) \quad and \quad N = \sqrt{\frac{2A_{12}^* + A_{33}^* - \sqrt{\Delta}}{2A_{11}^*}}(k\zeta) \qquad k = 1,2...8$$

If $\Delta = 0$ Then

$$F_k(y) = C_{k1}\cosh(Sy) + C_{k2}\sinh(Sy) + C_{k3}y\cosh(Sy) + C_{k4}y\sinh(Sy) + \Phi_k(y)$$

where

$$S = \sqrt[4]{\frac{A_{22}^*}{A_{11}^*}}(k\zeta) \qquad k = 1,2..8$$

If $\Delta < 0$ Then

$$F_k(y) = (C_{k1}\cos(Qy) + C_{k2}\sin(Qy))\sinh(Ry) + (C_{k3}\cos(Qy) + C_{k4}\sin(Qy))\cosh(Ry) + \Phi_k(y)$$

where

$$R = \sqrt{2\sqrt{\frac{A_{22}^*}{A_{11}^*}} + \frac{2A_{12}^* + A_{33}^*}{A_{11}^*}}\left(\frac{k\zeta}{2}\right) \quad and \quad Q = \sqrt{2\sqrt{\frac{A_{22}^*}{A_{11}^*}} - \frac{2A_{12}^* + A_{33}^*}{A_{11}^*}}\left(\frac{k\zeta}{2}\right) \quad k = 1,2..8$$

(12)

In Eq. (12) the functions $\Phi_k(y)$ (where k=1,2,…8) are the particular integral solutions which depend on the functions $f_i(y)$, $g_i(y)$, $s_i(y)$ (where i=1,2,3) only.

It can be observed that regardless of the DELTA sign, 32 coefficients C_{k1}−C_{k4} (where k=1,2,…8) are present in any of abovementioned solutions. For a given case, the sign of DELTA should be calculated first and consequently the proper solution for stress functions from Eq. (12) would be determined. It should be mentioned that for FG plates DELTA is always zero due to the isotropic properties of in-plane stiffness matrix. The 32 coefficients of C_{k1}−C_{k4} (where k=1,2,…8) are unknown at the present, but it is assumed that these coefficients are known. By taking this assumption into account and imposing the appropriate boundary conditions from Eq. (5) and solving the stress-strain constitutive equations, the in-plane displacements will be derived analytically as Eqs. (13) and (14)

$$
\begin{aligned}
u = & -\frac{\bar{u}}{L}x + f_{u_1}(y)\sin(\zeta x) + f_{u_2}(y)\sin(2\zeta x) + \\
& f_{u_3}(y)\sin(3\zeta x) + f_{u_4}(y)\sin(4\zeta x) + f_{u_5}(y)\sin(5\zeta x) + \\
& f_{u_6}(y)\sin(6\zeta x) + f_{u_7}(y)\sin(7\zeta x) + f_{u_8}(y)\sin(8\zeta x)
\end{aligned}
$$

where

$$
\begin{aligned}
f_{u_1} &= [A_{11}^* F_1^{''} - A_{12}^* (\zeta)^2 F_1 - \frac{\zeta^2}{4}(2 f_1 f_2 + 4 f_2 f_3 - 2\frac{B_{12}^* s_2^{'}}{\zeta^2} + 2\frac{B_{11}^* g_2}{\zeta})] \times \frac{1}{\zeta} \\
f_{u_2} &= [A_{11}^* F_2^{''} - A_{12}^* (2\zeta)^2 F_2 - \frac{\zeta^2}{4}(-4 f_3^2 - \frac{7}{4} f_2^2 + 4 f_1 f_3 - 4\frac{B_{11}^* g_1}{\zeta} + 4\frac{B_{11}^* g_3}{\zeta} \\
& + 2\frac{B_{12}^* s_1^{'}}{\zeta^2} - 2\frac{B_{12}^* s_3^{'}}{\zeta^2})] \times \frac{1}{2\zeta} \\
f_{u_3} &= [A_{11}^* F_3^{''} - A_{12}^* (3\zeta)^2 F_3 - \frac{\zeta^2}{4}(f_1 f_2 - 3 f_2 f_3 - 6\frac{B_{11}^* g_2}{\zeta} + 2\frac{B_{12}^* s_2^{'}}{\zeta^2})] \times \frac{1}{3\zeta} \\
f_{u_4} &= [A_{11}^* F_4^{''} - A_{12}^* (4\zeta)^2 F_4 - \frac{\zeta^2}{4}(\frac{3}{2} f_2^2 - f_3^2 - f_1^2 + 2 f_1 f_3 \\
& - 8\frac{B_{11}^* g_3}{\zeta} + 2\frac{B_{12}^* s_3^{'}}{\zeta^2})] \times \frac{1}{4\zeta} \\
f_{u_5} &= [A_{11}^* F_5^{''} - A_{12}^* (5\zeta)^2 F_5 - \frac{\zeta^2}{4}(5 f_2 f_3 - 3 f_2 f_1)] \times \frac{1}{5\zeta} \\
f_{u_6} &= [A_{11}^* F_6^{''} - A_{12}^* (6\zeta)^2 F_6 - \frac{\zeta^2}{4}(-\frac{9}{4} f_2^2 + 4 f_3^2 - 4 f_1 f_3)] \times \frac{1}{6\zeta} \\
f_{u_7} &= [A_{11}^* F_7^{''} - A_{12}^* (7\zeta)^2 F_7 - \frac{\zeta^2}{4}(-6 f_2 f_3)] \times \frac{1}{7\zeta} \\
f_{u_8} &= [A_{11}^* F_8^{''} - A_{12}^* (8\zeta)^2 F_8 - \frac{\zeta^2}{4}(-4 f_3^2)] \times \frac{1}{8\zeta}
\end{aligned}
\tag{13}
$$

The first term on the right hand side of Eq. (13) presents the prescribed uniform end shortening. The amplitude of the next eight terms evaluated at y=0 and $y=b_s$ (i.e., $f_{u_k}(y)\big|_{y=0}$ and $f_{u_k}(y)\big|_{y=b_s}$ $k=1,2,..8$) represents the local degrees of freedom u_{1k} and u_{2k}, respectively. It should be mentioned that by defining the degrees of freedom, as outlined above, the compatibility conditions will be ensured on the adjacent edges of two strips.

$$\upsilon = -(\frac{A_{21}^*}{A_{11}^*})\frac{\bar{u}}{L}y + I^{1\upsilon} + f_{\upsilon_1}\cos(\zeta x) + f_{\upsilon_2}\cos(2\zeta x) + f_{\upsilon_3}\cos(3\zeta x) + f_{\upsilon_4}\cos(4\zeta x) +$$
$$f_{\upsilon_5}\cos(5\zeta x) + f_{\upsilon_6}\cos(6\zeta x) + f_{\upsilon_7}\cos(7\zeta x) + f_{\upsilon_8}\cos(8\zeta x)$$
$$-(f_{\upsilon_1} + f_{\upsilon_2} + f_{\upsilon_3} + f_{\upsilon_4} + f_{\upsilon_5} + f_{\upsilon_6} + f_{\upsilon_7} + f_{\upsilon_8})\big|_{y=0} + \upsilon\big|_{x=y=0}$$

where

$$I^{1\upsilon} = \int_0^y [(\frac{A_{21}^*}{4A_{11}^*})\zeta^2(f_1^2 + \frac{5}{2}f_2^2 + 5f_3^2 - 2f_1f_3) - \frac{1}{8}(-f_1'f_3' + f_2'^2 + \frac{3}{2}f_1'^2 + f_3'^2)$$
$$-(\frac{A_{21}^*B_{12}^*}{2A_{11}^*})s_1']dy$$

$$f_{\upsilon_1} = -\frac{1}{1680\zeta}(1680A_{33}^*F_2'\zeta - 1680f_{u_1}' - 1470f_2f_3'\zeta + 1680f_3f_2'\zeta - 840f_1f_2'\zeta$$
$$+1260f_2f_1'\zeta - 840B_{33}^*g_2' - 840B_{33}^*s_2\zeta)$$

$$f_{\upsilon_2} = -\frac{1}{1680\zeta}(1680A_{33}^*F_2'\zeta - 840f_{u_2}' + 840f_3f_1'\zeta - 210f_1f_3'\zeta - 105f_2f_2'\zeta - 210f_3f_3'\zeta$$
$$-420f_1f_1'\zeta - 840B_{33}^*s_3\zeta - 420B_{33}^*g_3' + 840B_{33}^*s_1\zeta + 420B_{33}^*g_1')$$

$$f_{\upsilon_3} = -\frac{1}{1680\zeta}(1680A_{33}^*F_3'\zeta - 560f_{u_3}' - 140f_1f_2'\zeta - 140f_3f_2'\zeta + 140f_2f_3'\zeta - 490f_2f_1'\zeta$$
$$+840B_{33}^*s_2\zeta + 280B_{33}^*g_2')$$

$$f_{\upsilon_4} = -\frac{1}{1680\zeta}(1680A_{33}^*F_4'\zeta - 420f_{u_4}' + 105f_1f_1'\zeta - 105f_1f_3'\zeta - 525f_3f_1'\zeta + 105f_3f_3'\zeta$$
$$-210f_2f_2'\zeta + 840B_{33}^*s_3\zeta + 210B_{33}^*g_3')$$

$$f_{\upsilon_5} = -\frac{1}{1680\zeta}(1680A_{33}^*F_5'\zeta - 336f_{u_5}' - 168f_2f_3'\zeta + 126f_2f_1'\zeta + 84f_1f_2'\zeta - 252f_3f_2'\zeta)$$
$$-210f_2f_2'\zeta + 840B_{33}^*s_3\zeta + 210B_{33}^*g_3')$$

$$f_{\upsilon_6} = -\frac{1}{1680\zeta}(1680A_{33}^*F_6'\zeta - 280f_{u_6}' + 70f_1f_3'\zeta + 105f_2f_2'\zeta - 210f_3f_3'\zeta + 140f_3f_1'\zeta)$$

$$f_{\upsilon_7} = -\frac{1}{1680\zeta}(1680A_{33}^{*}F_7'\zeta - 240\,f_{u_7}' + 120\,f_3 f_2'\zeta + 90\,f_2 f_3'\zeta)$$
$$f_{\upsilon_8} = -\frac{1}{1680\zeta}(1680A_{33}^{*}F_8'\zeta - 210\,f_{u_6}' + 105\,f_3 f_3'\zeta) \tag{14}$$

The first term on the right hand side of Eq. (14) describes the transverse in-plane expansion of the strip, which translates to the Poisson's ratio effect for an isotropic material. The second term (i.e., $I^{1\upsilon}$) describes the transverse in-plane movement of the lines parallel to *x*-axis across a strip. This movement, which is constant along a given line, varies from a minimum value of zero at edge $y=0$ to its maximum value at the edge $y=b_s$. The next eight terms describe the in-plane waviness of the lines which lie parallel to x-axis. The amplitude of these terms evaluated at $y=0$ and $y=b_s$ (i.e., $f_{\upsilon_k}(y)\big|_{y=0}$ and $f_{\upsilon_k}(y)\big|_{y=b_s}$, $k=1,2,..8$) represents the local degrees of freedom υ_{1k} and υ_{2k}, respectively. Finally, the eleventh term (which is equivalent to $-(f_{\upsilon 1}+f_{\upsilon 2}+f_{\upsilon 3}+f_{\upsilon 4}+f_{\upsilon 5}+f_{\upsilon 6}+f_{\upsilon 7}+f_{\upsilon 8})|_{y=0}$) and the twelfth term on the right hand side of Eq. (14) represents values which remain constant at all points on a given strip. The existence of the eleventh term on the right hand side of Eq. (14) allows the point ($x=0$, $y=0$) to be treated as a reference point in terms of its deflection being connected to another strip or being restrained.

It is noted that in the above equations (i.e., Eqs. (13), (14)), functions $F_k(y)$ ($k=1,2,\ldots 8$) are not yet fully known, due to the coefficients C_{k1}–C_{k4} (where $k=1,2,\ldots 8$)) being unknown. These coefficients are obtained by treating them as unknown, and solving for them whiles all other parameters, including all DOFs $u_{1k}, \upsilon_{1k}, u_{2k}, \upsilon_{2k}, w_{1i}, w_{1\frac{1}{4}i}, w_{1\frac{3}{4}i}, w_{2i}, \varphi_{x_{1i}}, \varphi_{x_{1\frac{1}{2}i}}, \varphi_{x_{2i}}, \varphi_{y_{1i}}, \varphi_{y_{1\frac{1}{2}i}}, \varphi_{y_{2i}}$ ($i=1,2,3$, $k=1,2,\ldots 8$), are assumed to be known. In this process, the following set of equations should be solved analytically.

$$\begin{cases} f_{u_k}(y)\big|_{y=0} = u_{1k} \\ f_{u_k}(y)\big|_{y=b_s} = u_{2k} \end{cases}, \quad \begin{cases} f_{\upsilon_k}(y)\big|_{y=0} = \upsilon_{1k} \\ f_{\upsilon_k}(y)\big|_{y=b_s} = \upsilon_{2k} \end{cases} \quad Where \quad k=1,2,...,8 \tag{15}$$

It should be mentioned that in the set of 32 equations presented in Eq. (15), all the equations are linear with respect to the undetermined coefficients of C_{k1}–C_{k4} (where $k=1,2,\ldots 8$)). Thus, by implementing an analytical scheme, the 32 coefficients of C_{k1}–C_{k4} (where $k=1,2,\ldots 8$)) are explicitly evaluated in terms of the degrees of freedom and other strip constants.

Having derived the in-plane displacement functions (i.e., u and υ), the mid-plane strain and curvatures with respect to the von Karman's assumptions can be derived as follow

$$\{\varepsilon_l\}^T = \left\{\frac{\partial u}{\partial x}, \frac{\partial \upsilon}{\partial y}, \frac{\partial u}{\partial y} + \frac{\partial \upsilon}{\partial x}\right\}, \{\varepsilon_{nl}\}^T = \left\{\frac{1}{2}\left(\frac{\partial w}{\partial x}\right)^2, \frac{1}{2}\left(\frac{\partial w}{\partial y}\right)^2, \frac{\partial w}{\partial x}\frac{\partial w}{\partial y}\right\}$$
$$(where \;\; \varepsilon = \varepsilon_l + \varepsilon_{nl}) \tag{16}$$
$$\phi^T = \left\{\frac{\partial \varphi_x}{\partial x}, \frac{\partial \varphi_y}{\partial y}, \frac{\partial \varphi_x}{\partial y} + \frac{\partial \varphi_y}{\partial x}\right\}, \lambda^T = \left\{\varphi_x + \frac{\partial w}{\partial x}, \varphi_y + \frac{\partial w}{\partial y}\right\}$$

The strain energy for the FG finite strip in terms of mid-plane strains and curvatures is presented as follow

$$V_s = \frac{1}{2}\iint (\{\varepsilon_l\}^T[A]\{\varepsilon_l\} + 2\{\varepsilon_l\}^T[B]\{\phi\} + \{\phi\}^T[D]\{\phi\} + 2\{\varepsilon_{nl}\}^T[A]\{\varepsilon_l\} + \{\varepsilon_{nl}\}^T[A]\{\varepsilon_{nl}\} + 2\{\varepsilon_{nl}\}^T[B]\{\phi\} + (SCF)(\{\lambda\}^T[E]\{\lambda\}))dxdy \tag{17}$$

Where [*D*] is the out-of-plane stiffness matrix, [*E*] is the shear stiffness matrix through the thickness and SCF is the shear correction factor.

By invoking the principle of minimum potential energy the strip equilibrium equations can be obtained and subsequently rearranged into the non-linear stiffness matrix of the strip. Once strip equilibrium equations are determined for all strips, the equations are assembled to form a set of global equilibrium equations (i.e., a set of global stiffness equations) for the whole structure. After the application of any appropriate zero-displacement boundary conditions, the global equilibrium equations are then solved using the Newton-Raphson (N-R) iterative procedure.

Once the global equilibrium equations are solved and the degrees of freedom are found for a particular prescribed end shortening and pressure loading, it is possible to calculate the out-of plane displacement w and rotations with respect to x, y axes in any finite strip using Eq. (8) directly. The calculation of in-plane displacements u and v is achieved after finding $F_k(y)$, $f_{u_k}(y)$ and $f_{v_k}(y)$. Having obtained the functions $F_k(y)$, the average stresses at any point of the strip is known by Eqs. (7)-(9).

By integrating the stress resultants along and across a given FG strip, the total mean force acting on a strip will be derived as follows

$$P = \frac{\int_0^L \int_0^{b_s} N_x dxdy}{L} \tag{18}$$

It is to be noted that the average in-plane stresses are evaluated by solving the von Karman's compatibility equation on a FG strip and the derived in-plane displacement functions will satisfy the mentioned equation. Therefore, as the in-plane displacements are continuous along an adjacent edge of two FG strips, the average in-plane stresses will be compatible on this edge as a result of von Karman's compatibility equation satisfaction.

5. Semi-energy finite strip formulation using CLPT

As mentioned in the previous section, the FG strip is clamped out-of-plane at both ends (i.e., at end x=0 and L), and is subjected to a uniform end shortening $\bar{u}$ at end x=L only. Therefore, the boundary conditions at loaded ends of the FG finite strip are summarized as Eq. (19) with CLPT assumptions.

$$w = \frac{\partial w}{\partial x} = N_{xy} = 0 \qquad at\ x = 0\ \&\ L \qquad and \qquad u = \begin{cases} 0 & at\ x = 0 \\ -\bar{u} & at\ x = L \end{cases} \tag{19}$$

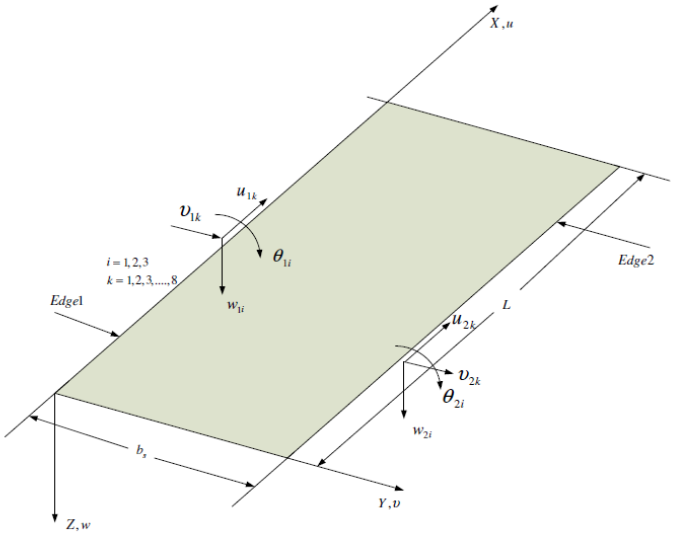

Fig. 3 Degrees of freedom for the FG finite strip with CLPT assumptions.

The Von Karman's compatibility equation for large deflections of arbitrary lay-up laminated plates as given in Ref. (Chai 1989) is modified as Eq. (20) for FG plates in which the CLPT assumptions are incorporated

$$\nabla^4 F = A_{22}^* \frac{\partial^4 F}{\partial x^4} + (2A_{12}^* + A_{33}^*) \frac{\partial^4 F}{\partial x^2 \partial y^2} + A_{11}^* \frac{\partial^4 F}{\partial y^4} = (\frac{\partial^2 w}{\partial x \partial y})^2 - (\frac{\partial^2 w}{\partial x^2})(\frac{\partial^2 w}{\partial y^2}) + B_{21}^* \frac{\partial^4 w}{\partial x^4} + (B_{11}^* + B_{22}^* - 2B_{33}^*) \frac{\partial^4 w}{\partial x^2 \partial y^2} + B_{12}^* \frac{\partial^4 w}{\partial y^4} \tag{20}$$

In this version of the semi-energy finite strip approach which is suitable for the post-buckling analysis of thin FG plate structures, the out-of-plane displacement field of the finite strip is the only displacement which is postulated by a deflected form due to the application of classic laminated plate theory (CLPT). The following function is found to be suitable to represent the out-of-plane displacement field for the developed semi-energy finite strip formulation

$$w = \sum_{i=1}^{N} f_{wi}(y) \sin(i\zeta x) \sin(\zeta x) \quad , \quad \zeta = \frac{\pi}{L}, \ \eta = \frac{y}{b_s}$$
$$f_{wi} = (1 - 3\eta^2 + 2\eta^3) w_{1i} + b_s(\eta - 2\eta^2 + \eta^3)\theta_{1i} + (3\eta^2 - 2\eta^3) w_{2i} + b_s(\eta^3 - \eta^2)\theta_{2i} \tag{21}$$

In the above expression w_{1i}, θ_{1i}, w_{2i}, θ_{2i} (where i = 1..N) are the undetermined out-of-plane nodal displacement parameters along edges 1 and 2 of the FG strip, respectively. The degrees of freedom (DOF), called nodal displacement parameters, are depicted in Fig. 3 for a FG finite strip with CLPT assumptions. Again, the investigation on the sensitivity of the semi-energy FSM analysis to the number of harmonic terms in out-of-plane deflection series has revealed that, the early stages of the post-buckling behavior of thin FG plates can be predicted with a very good accuracy by using three first harmonic terms (i.e., N=3 in Eq. (21)).

Similar to the procedure followed in the previous section with respect to the Von-Karman solution related to the FSDT case, the out-of-plane displacement *w* is then substituted into the Von-Karman's compatibility equation in order to find the corresponding in-plane displacement functions. In this process, the stress function *F* may be considered as Eq. (9). Substituting *F* from Eq. (9) and *w* from Eq. (21) into Eq. (20), a set of fourth-order ordinary differential equations will be achieved as Eq. (22).

$$\begin{cases} A_{11}^{*}F_0^{""} = \zeta^2 \Psi_0\left(f_{w1}, f_{w2}, f_{w3}\right) \\ A_{11}^{*}F_k^{""} - (k\zeta)^2\left(2A_{12}^{*} + A_{33}^{*}\right)F_k^{"} + (k\zeta)^4 A_{22}^{*}F_k = \zeta^2\Psi_k\left(f_{w1}, f_{w2}, f_{w3}\right) \end{cases} \quad (22)$$

where $\mathrm{k} = 1,2,...,8$

It is also noted that Ψ_0, Ψ_1, Ψ_2 … Ψ_8 are known functions and can be derived analytically. With the establishment of the out-of-plane displacement field according to Eq. (21) and driving governing equations according to the above-mentioned ordinary differential equations, the rest of the analysis concerning to find in-plane displacement fields is carried out in the same manner as that already described with respect to the semi-energy finite strip method using first order shear deformation theory. In this process, the in-plane displacement fields will be obtained as follow

$$u = -\frac{\bar{u}}{L}x + f_{u_1}(y)\sin(\zeta x) + f_{u_2}(y)\sin(2\zeta x) + f_{u_3}(y)\sin(3\zeta x) +$$
$$f_{u_4}(y)\sin(4\zeta x) + f_{u_5}(y)\sin(5\zeta x) + f_{u_6}(y)\sin(6\zeta x) +$$
$$f_{u_7}(y)\sin(7\zeta x) + f_{u_8}(y)\sin(8\zeta x)$$

where

$$f_{u_1} = (A_{11}^{*}F_1^{"} - A_{12}^{*}(\zeta)^2 F_1 - \frac{\zeta^2}{4}(2f_{w1}f_{w2} + 4f_{w2}f_{w3} + \frac{2}{\zeta^2}B_{12}^{*}f_{w2}^{"}$$
$$-2B_{11}^{*}f_{w2})) \times \frac{1}{\zeta}$$

$$f_{u_2} = (A_{11}^{*}F_2^{"} - A_{12}^{*}(2\zeta)^2 F_2 - \frac{\zeta^2}{4}(\frac{2}{\zeta^2}B_{12}^{*}f_{w3}^{"} + 8B_{11}^{*}f_{w1} - 8B_{11}^{*}f_{w3}$$
$$-\frac{2}{\zeta^2}B_{12}^{*}f_{w1}^{"} - 4{f_{w3}}^2 - \frac{7}{4}{f_{w2}}^2 + 4f_{w1}f_{w3})) \times \frac{1}{2\zeta}$$

$$f_{u_3} = (A_{11}^{*}F_3^{"} - A_{12}^{*}(3\zeta)^2 F_3 - \frac{\zeta^2}{4}(18B_{11}^{*}f_{w2} - \frac{2}{\zeta^2}B_{12}^{*}f_{w2}^{"} + f_{w1}f_{w2}$$
$$-3f_{w3}f_{w2})) \times \frac{1}{3\zeta}$$

$$f_{u_4} = (A_{11}^{*}F_4^{"} - A_{12}^{*}(4\zeta)^2 F_4 - \frac{\zeta^2}{4}(32B_{11}^{*}f_{w3} - \frac{2}{\zeta^2}B_{12}^{*}f_{w3}^{"} + 2f_{w1}f_{w3} +$$

$$\frac{3}{2} f_{w2}{}^{2} - f_{w3}{}^{2} - f_{w1}{}^{2})) \times \frac{1}{4\zeta}$$

$$f_{u_5} = (A_{11}^{*} F_5^{''} - A_{12}^{*} (5\zeta)^2 F_5 - \frac{\zeta^2}{4}(5 f_{w2} f_{w3} - 3 f_{w2} f_{w1})) \times \frac{1}{5\zeta}$$

$$f_{u_6} = (A_{11}^{*} F_6^{''} - A_{12}^{*} (6\zeta)^2 F_6 - \frac{\zeta^2}{4}(-\frac{9}{4} f_{w2}{}^{2} + 4 f_{w3}{}^{2} - 4 f_{w1} f_{w3})) \times \frac{1}{6\zeta}$$

$$f_{u_7} = (A_{11}^{*} F_7^{''} - A_{12}^{*} (7\zeta)^2 F_7 - \frac{\zeta^2}{4}(-6 f_{w2} f_{w3})) \times \frac{1}{7\zeta}$$

$$f_{u_8} = (A_{11}^{*} F_8^{''} - A_{12}^{*} (8\zeta)^2 F_8 - \frac{\zeta^2}{4}(-4 f_{w3}{}^{2})) \times \frac{1}{8\zeta} \tag{23}$$

$$\upsilon = -(\frac{A_{21}^{*}}{A_{11}^{*}}) \frac{\bar{u}}{L} y + I^{1\upsilon} + f_{\upsilon_1} \cos(\zeta x) + f_{\upsilon_2} \cos(2\zeta x) + f_{\upsilon_3} \cos(3\zeta x)$$
$$+ f_{\upsilon_4} \cos(4\zeta x) + f_{\upsilon_5} \cos(5\zeta x) + f_{\upsilon_6} \cos(6\zeta x) + f_{\upsilon_7} \cos(7\zeta x) + f_{\upsilon_8} \cos(8\zeta x)$$
$$-(f_{\upsilon_1} + f_{\upsilon_2} + f_{\upsilon_3} + f_{\upsilon_4} + f_{\upsilon_5} + f_{\upsilon_6} + f_{\upsilon_7} + f_{\upsilon_8})\Big|_{y=0} + \upsilon\Big|_{x=y=0}$$

where

$$I^{1\upsilon} = \int_0^y ((\frac{A_{21}^{*}}{4A_{11}^{*}})\zeta^2 (f_{w1}^2 + \frac{5}{2} f_{w2}^2 + f_{w3}^2 - f_{w1} f_{w3})$$
$$-\frac{1}{8}(-f_{w1}^{'} f_{w3}^{'} + f_{w2}^{'}{}^{2} + \frac{3}{2} f_{w1}^{'}{}^{2} + f_{w3}^{'}{}^{2}) + \frac{1}{2}(\frac{A_{21}^{*} B_{12}^{*}}{A_{11}^{*}}) f_{w1}^{''} - \frac{1}{2} B_{22}^{*} f_{w1}^{''}) dy$$

$$f_{\upsilon_1} = \frac{A_{11}^{*}}{(\zeta)^2} F_1^{'''} - (A_{12}^{*} + A_{33}^{*}) F_1^{'} - \frac{1}{8} f_{w2} f_{w3}^{'} - \frac{5}{4} f_{w2} f_{w1}^{'} - 2 f_{w3} f_{w2}^{'}$$
$$-\frac{1}{2\zeta^2} B_{12}^{*} f_{w2}^{'''} + \frac{1}{2} B_{11}^{*} f_{w2}^{'} - B_{33}^{*} f_{w2}^{'}$$

$$f_{\upsilon_2} = \frac{A_{11}^{*}}{(2\zeta)^2} F_2^{'''} - (A_{12}^{*} + A_{33}^{*}) F_2^{'} + \frac{9}{32} f_{w2} f_{w2}^{'} - \frac{3}{4} f_{w3} f_{w1}^{'} + \frac{1}{2} f_{w1} f_{w1}^{'}$$
$$-\frac{1}{8} f_{w1} f_{w3}^{'} + \frac{5}{8} f_{w3} f_{w3}^{'} + B_{33}^{*} f_{w3}^{'} + B_{33}^{*} f_{w1}^{'} - \frac{1}{2} B_{11}^{*} f_{w1}^{'} + \frac{1}{8\zeta^2} B_{12}^{*} f_{w1}^{'''}$$
$$-\frac{1}{8\zeta^2} B_{12}^{*} f_{w3}^{'''} + \frac{1}{2} B_{11}^{*} f_{w3}^{'}$$

$$f_{\upsilon_3} = \frac{A_{11}^{*}}{(3\zeta)^2} F_3^{'''} - (A_{12}^{*} + A_{33}^{*}) F_3^{'} + \frac{1}{18} f_{w1} f_{w2}^{'} + \frac{19}{72} f_{w2} f_{w1}^{'} + \frac{1}{6} f_{w3} f_{w2}^{'}$$

$$+\frac{1}{18\zeta^2}B_{12}^{*}f_{w2}^{'''}-\frac{1}{2}B_{11}^{*}f_{w2}^{'}+B_{33}^{*}f_{w2}^{'}$$

$$f_{\upsilon_4}=\frac{A_{11}^{*}}{(4\zeta)^2}F_4^{'''}-(A_{12}^{*}+A_{33}^{*})F_4^{'}+\frac{5}{56}f_{w2}f_{w2}^{'}+\frac{9}{32}f_{w3}f_{w1}^{'}-\frac{1}{32}f_{w1}f_{w1}^{'}$$

$$+\frac{1}{32}f_{w1}f_{w3}^{'}-\frac{1}{32}f_{w3}f_{w3}^{'}-\frac{1}{2}B_{11}^{*}f_{w3}^{'}+B_{33}^{*}f_{w3}^{'}+\frac{1}{32\zeta^2}B_{12}^{*}f_{w3}^{'''}$$

$$f_{\upsilon_5}=\frac{A_{11}^{*}}{(5\zeta)^2}F_5^{'''}-(A_{12}^{*}+A_{33}^{*})F_5^{'}-\frac{9}{200}f_{w2}f_{w1}^{'}+\frac{1}{10}f_{w3}f_{w2}^{'}+\frac{1}{20}f_{w2}f_{w3}^{'}$$

$$-\frac{1}{50}f_{w1}f_{w2}^{'}$$

$$f_{\upsilon_6}=\frac{A_{11}^{*}}{(6\zeta)^2}F_6^{'''}-(A_{12}^{*}+A_{33}^{*})F_6^{'}-\frac{1}{32}f_{w2}f_{w2}^{'}-\frac{1}{18}f_{w3}f_{w1}^{'}-\frac{1}{72}f_{w1}f_{w3}^{'}$$

$$+\frac{5}{72}f_{w3}f_{w3}^{'}$$

$$f_{\upsilon_7}=\frac{A_{11}^{*}}{(7\zeta)^2}F_7^{'''}-(A_{12}^{*}+A_{33}^{*})F_7^{'}-\frac{2}{49}f_{w3}f_{w2}^{'}-\frac{9}{932}f_{w2}f_{w3}^{'}$$

$$f_{\upsilon_8}=\frac{A_{11}^{*}}{(8\zeta)^2}F_8^{'''}-(A_{12}^{*}+A_{33}^{*})F_8^{'}-\frac{1}{32}f_{w3}f_{w3}^{'} \tag{24}$$

It is noted that the all parameters in Eqs. (23) and (24) have the same meanings as those discussed earlier with respect to FSDT semi-energy FSM. One of the most important differences between the two methods (i.e., FSDT semi-energy FSM and CLPT semi-energy FSM) lies in the manner that the finite strip strain energy is computed for different methods. That is to say, in the classic laminated plate theory the shear strain energy at the thickness is assumed to be zero whilst in the first order shear deformation theory, the shear strain energy through the thickness is taken into account. Consequently strain energy for CLPT assumptions (by putting λ=0 in the Eq. (17)) will be derived as follows

$$V_s=\frac{1}{2}\iint(\{\varepsilon_l\}^T[A]\{\varepsilon_l\}+2\{\varepsilon_l\}^T[B]\{\phi\}+\{\phi\}^T[D]\{\phi\}+2\{\varepsilon_{nl}\}^T[A]\{\varepsilon_l\}$$
$$+\{\varepsilon_{nl}\}^T[A]\{\varepsilon_{nl}\}+2\{\varepsilon_{nl}\}^T[B]\{\phi\})dxdy \tag{25}$$

Where

$$[\phi]^T=\left\{-\frac{\partial^2 w}{\partial x^2},-\frac{\partial^2 w}{\partial y^2},-2\frac{\partial^2 w}{\partial x\partial y}\right\} \tag{26}$$

Again, by invoking the principle of minimum potential energy the strip equilibrium equations, and subsequently the global equilibrium equations are obtained for the whole structure.

6. Full-energy finite strip formulation using CLPT

In order to check the validity and numerical efficiency of the developed CLPT semi-energy FSM, a CLPT full-energy FSM based on Ovesy's approach (Ovesy and Ghannadpour 2007) is implemented in the current work. The main difference between the semi-energy and the full-energy methods lies on the fact that in the full-energy method, the in-plane displacements are postulated in addition to postulating a deflected form for the out-of-plane displacement by the appropriate deflected forms from the commencement of analysis as follows

$$u = -\frac{\bar{u}}{L}x + \sum_{i=1}^{8}((1-\eta)u_{1i} + \eta u_{2i})\sin(i\zeta x)$$

$$\upsilon = \frac{A_{12}}{A_{22}}\frac{\bar{u}}{L}y + \sum_{i=0}^{8}((1-\eta)\upsilon_{1i} + \eta\upsilon_{2i})\cos(i\zeta x)$$

$$w = \sum_{i=1}^{3}((1-3\eta^2+2\eta^3)w_{1\mathrm{i}} + \mathrm{b_s}(\eta-2\eta^2+\eta^3)\theta_{1\mathrm{i}} + (3\eta^2-2\eta^3)w_{2\mathrm{i}} + \mathrm{b_s}(\eta^3-\eta^2)\theta_{2\mathrm{i}})\sin(i\zeta x)\sin(\zeta x) \tag{27}$$

The rest of the analysis is carried out in the same manner as that already described with respect to the semi-energy FSM.

7. Numerical results and discussions

FG rectangular plates with loaded ends clamped out-of-plane and with the unloaded edges simply supported out-of-plane and free to move in-plane are considered. The set of FG materials considered is alumina and aluminum. Young's modulus and Poisson's ratio were selected as being 70 GPa and 0.3 for aluminum, and 380 GPa and 0.3 for alumina, respectively. In all cases, the bottom surface is assumed to be metal (aluminum) and the top surface is assumed to be pure ceramic (alumina). The results are presented in terms of non-dimensional coefficients as follows

$$P^* = -\frac{10PL}{E_t h^3} \quad , \quad U^* = 1000\frac{\bar{u}}{L} \quad , \quad W^* = \frac{w_{center}}{h} \quad , \quad K = \frac{10P_{cr}L}{E_t h^3}$$

$$P^{**} = -\frac{Pb}{\pi^2 D_{11}} \quad , \quad U^{**} = \frac{\bar{u}b^2 A_{11}}{\pi^2 L D_{11}} \tag{28}$$

Where E_t is alumina's Young modulus, P_{cr} is the total critical force acting on the plate in buckling point and D_{11}, A_{11} are the members of flexural and in-plane stiffness matrices, respectively.

7.1 Buckling behavior of FG plates

The first step is to investigate the buckling behavior of FG plates using Rayleigh-Ritz approach based on CLPT assumption. To achieve this goal, the variation of buckling load capacity of FG

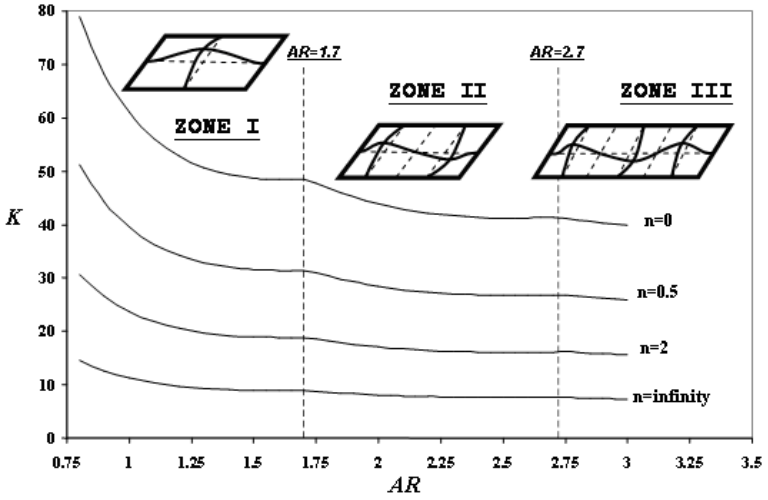

Fig. 4 Garland curves concerned with FG plates

plates with respect to aspect ratio is examined. It is noted that aspect ratio of a rectangular plate is defined as the length to width ratio (i.e., *L/b*) and is denoted as AR in this paper. It is assumed that the width of plate is *b*=100 mm and thickness *h* is equal to 1 mm. The variation of non-dimensional buckling coefficient *K* with aspect ratio of rectangular FG plate for different values of volume fraction index (i.e., *n*) is depicted in Fig. 4. The volume fraction values of *n*=0 and *n*=∞ correspond to two extreme cases of pure ceramic and pure metal materials, respectively. Therefore, the coupling effects between in-plane loads and out-of-plane moments and curvatures will be vanished. For the cases of *n*=0.5 and *n*=2 the related garland curves with regard to buckling performance of FG plates is also included in Fig. 4. It can be seen that the garland curves concerned with the mentioned volume fraction values lie between the curves related to extreme cases of *n*=0, ∞. Having analyzed the FG plates with different values of volume fraction index, it is concluded that for each specified aspect ratio the buckling coefficient of FG plate with an arbitrary volume fraction index is bounded among the buckling coefficient values corresponding to two limit cases of *n=0* and *n*=∞. In addition, all the curves depicted in Fig. 4 are demonstrating sudden changes in curvature at identical aspect ratios. In fact these changes are related to change in buckling mode shape of FG plate. Moreover, each curve is divided into three zones. By checking the buckling mode shapes it is revealed that each mode is constructed of one half waves in transverse direction and one, two, three and more half waves in longitudinal direction of FG plate. Therefore, each zone specified in Fig. 4 is concerned with the number of half waves in longitudinal direction of FG plate. As the loaded ends of FG plate are clamped out-of-plane a minimum buckling coefficient and related natural half-wave length may not be evaluated. It has been shown that for an isotropic plate, transition between *m* to (*m*+1) half waves (i.e., *m*=1,2,3…) in axial direction will take place at the aspect ratios equal to $\sqrt{m(m+2)}$ (Allen and Bulson, 1980). Similarly, for the extreme cases of *n=0*, ∞ as the FGM plates, a transition between one half wave to two half waves in length is experienced at AR of approximately 1.7 (i.e., $AR=\sqrt{3}$). Moreover, the transition from two half waves to three half waves for the cases of *n=0*, ∞ have seen to occur at AR of approximately 2.7 (i.e., $AR=\sqrt{8}$). It would be remarkable to note that;

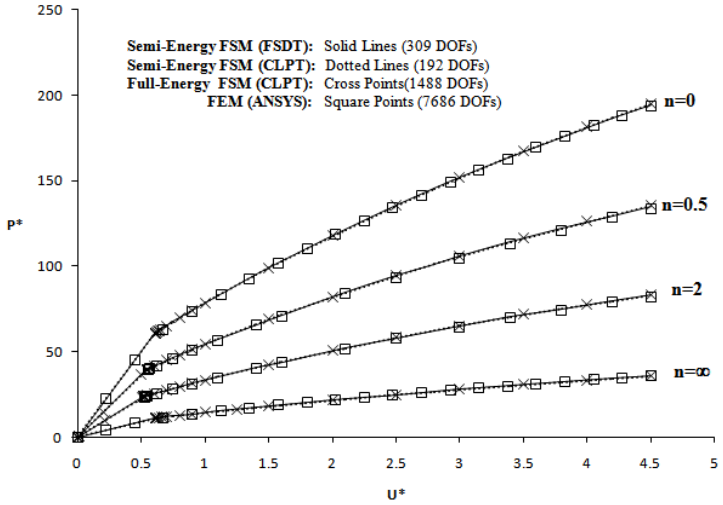

Fig. 5 Variations of non-dimensional load versus dimensionless end- shortening for square thin FG plates (L/h=100) with various volume fraction index

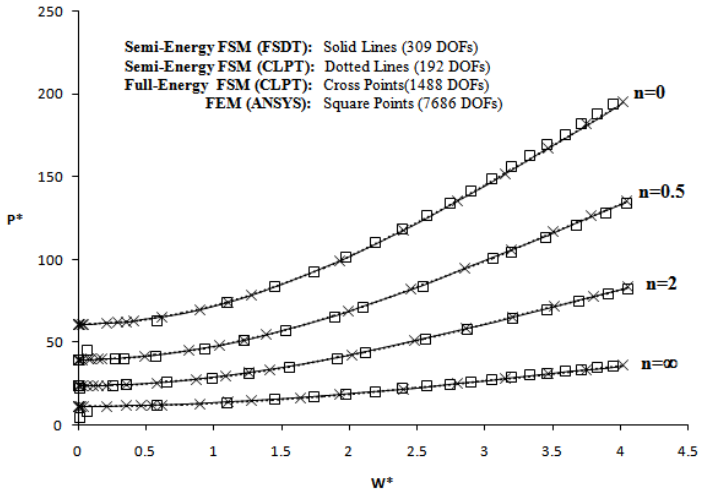

Fig. 6 Variations of non-dimensional load versus dimensionless out-of-plane central deflection for square thin FG plates (L/h=100) with various volume fraction index

although, the FG plates with n=0.5 and 2 have a type of material properties including coupling between in-plane and out-of-plane loads and deformations, the transition of mode shape for these FG plates have taken place in almost the same aspect ratios as those correspond to the aforementioned pure material cases. Therefore, the effects of mentioned coupling on the transition point may be negligible.

7.2 Post-buckling behavior of FG plates

The second step is to investigate the post-buckling behavior of square FG plates subject to a

uniform end shortening $\bar{u}$ at one end only. The thickness of the plates is kept equal to 1 mm, and the length to thickness ratios are varied as L/h=100, L/h=40, L/h=20, L/h=10 and L/h=5 in order to investigate plates with different relative thicknesses. A set of convergence studies concerning the required number of strips that tends to a converged post-buckling solution has been carried out. The convergence studies have revealed that a total number of 8 finite strips (corresponding to 309 and 192 DOFs in the case of semi-energy FSDT and CLPT FSM, respectively) and a total number of 64 finite strips (corresponding to 1488 DOFs in the case of full-energy FSM) will produce converged post-buckling solutions for the FG plates assumed in this paper. It should be mentioned that for semi-energy FSM analyses based on the concept of FSDT, the shear correction factor is assumed to be 5/6 for (n=0 & ∞) and 4/6 for (n=0.5 & 2).

In addition to the semi-energy and full-energy finite strip analyses, a finite element study is also performed in this paper. The FEM analysis has been carried out using general purpose ANSYS 11 software. The shell element (SHELL99) of the ANSYS library has been used. This element has eight nodes and each node incorporates six degrees of freedom. Within ANSYS software, the buckling analysis is a two-pass analysis. The first pass is a linear static analysis which determines the stresses for a given reference set of loads. The second pass is an eigen-value analysis which provides the results in terms of load factors (eigen-values) and mode shapes (eigen-vectors). Having obtained the mode shapes from an eigen value analysis in the manner described above, they are then used as postulated imperfections in order to perform an iterative nonlinear post-buckling analysis. In this process, the corresponding mode shape is scaled by a small factor and the geometry of the structure is then updated by using scaled mode shape as an imperfection. Within nonlinear FEM analysis, the postulation of an imperfection is a necessary step if the post-buckling path after bifurcation point is sought. The convergence study has revealed that a mesh arrangement composed of 400 square elements with the uniform size, for the FEM analysis is perfectly acceptable. It means that a total number of 7686 DOFs are used in FEM analysis. It is noted that the stiffness matrices of FG shell elements were computed outside of ANSYS environment and then entered into the software through user input real constants.

The variation of load factor P^* with dimensionless end-shortening U^*, and the variation of load factor P^* with dimensionless central deflection W^* for the very thin plate with L/h=100 are depicted in Figs. 5 and 6, respectively. Beside the presentation of the results obtained from the semi-energy FSM using FSDT and CLPT, the results obtained from finite element method and full-energy FSM are also presented for further validation.

It is clearly seen in Figs. 5 and 6 that for all volume fraction indexes, the four sets of results compare very closely and hence that the present approaches for the post-buckling behaviours of thin FG plates under uniform end shortening are verified. It is noted that due to the high length to thickness ratio of plate, the effect of shear strain energy at the thickness is negligible, and thus the results obtained from CLPT theory (full-energy CLPT-FSM and semi-energy CLPT-FSM) and FSDT theory (i.e., FEM and semi-energy FSDT-FSM) are very close. It is also seen in Figs. 5 and 6 that for a given value of loading, among plates with different combinations of materials, the plate made up of pure aluminum (i.e., n=infinity) encounters the largest end-shortening and central deflection, whilst the smallest end-shortening and central deflection are encountered by the plate made up of pure alumina (i.e., n=0). This is due to the fact that the former plate has the lowest Young's modulus (i.e., E=70 GPa), in contrast to the highest Young's modulus of the latter plate (i.e., E=380 GPa). Moreover, from the computational economy point of view it is worth mentioning that the semi-energy FSM has incorporated very lower number of degrees of freedom (i.e., 309DOFs in semi-energy FSDT-FSM and 192DOFs in semi-energy CLPT-FSM) compared

to those of full-energy FSM (1488DOFs) and FEM (7686DOFs), thus the computational advantage of the developed semi-energy FSM is revealed.

For the plates with L/h=40 & 20, the results obtained from the current semi-energy FSM analyses based on both CLPT and FSDT theories as well as FEM analyses are presented in Figs. 7 and 8, respectively. It is clearly seen that the semi-energy FSM results obtained by the application of FSDT theory are very close to those obtained by FEM analysis. The differences between the FSM results obtained from CLPT theory and FSDT theory are due to the fact that for relatively thick plates the through-the-thickness shear strain energy is no longer negligible and thus needs to be accounted for. However, it is worth mentioning that at the expense of some loss in the accuracy,

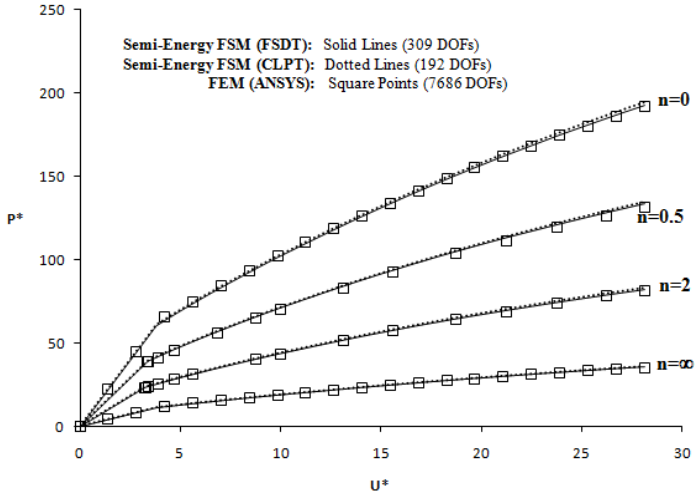

Fig. 7 Variations of non-dimensional load versus dimensionless end- shortening for square FG plates (L/h=40) with various volume fraction index

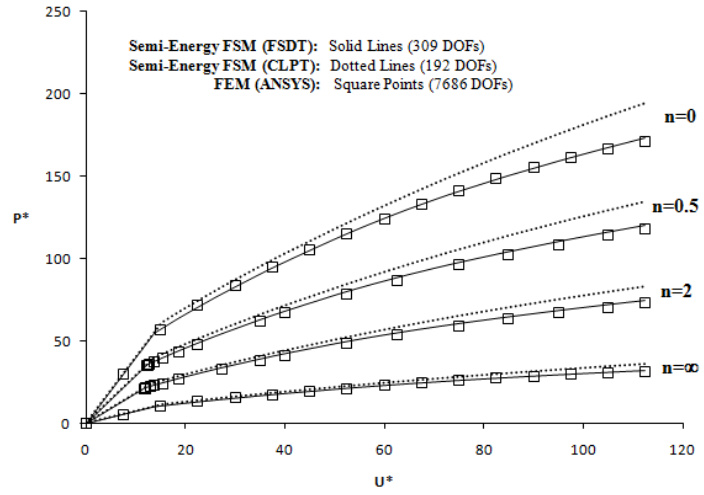

Fig. 8 Variations of non-dimensional load versus dimensionless end- shortening for square FG plates (L/h=20) with various volume fraction index

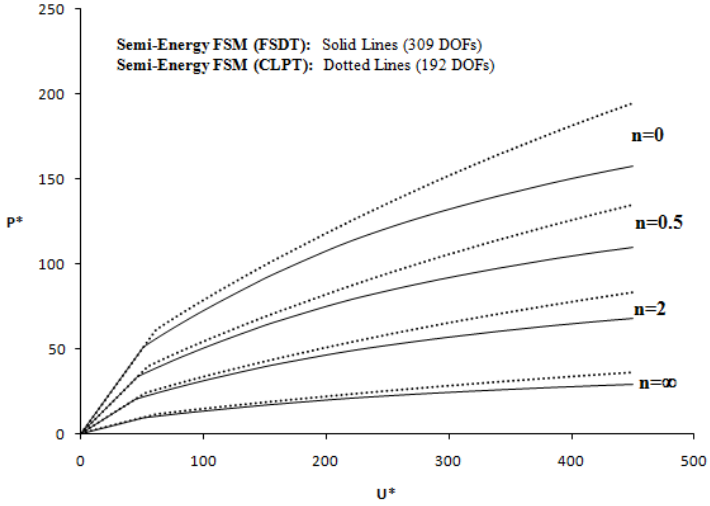

Fig. 9 Variations of non-dimensional load versus dimensionless end- shortening for square FG plates (L/h=10) with various volume fraction index

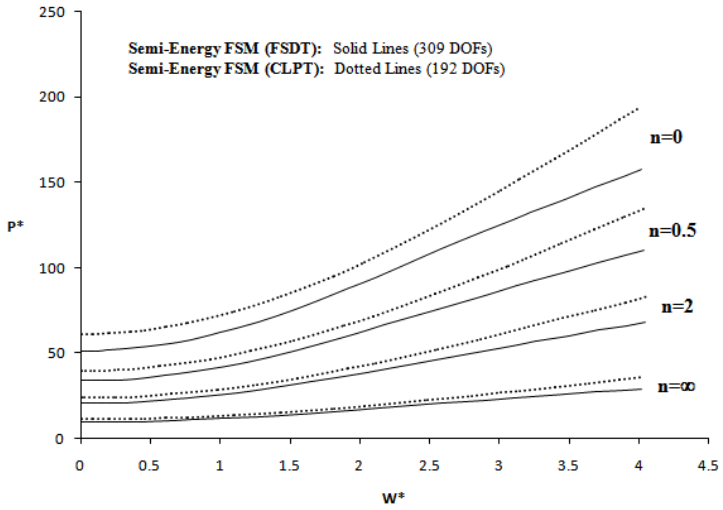

Fig. 10 Variations of non-dimensional load versus dimensionless out-of-plane central deflection for square thin FG plates (L/h=10) with various volume fraction index

the semi-energy CLPT-FSM analysis requires a significantly lower number of degrees of freedom (i.e., 192 DOF) compared to those required by the semi-energy FSDT-FSM analysis (i.e., 309 DOF). Therefore, if the computational economy is concerned the CLPT-FSM post-buckling analysis may be suggested by obviously compromising on the precision of results.

The effects of through-the-thickness shear strains are further investigated in Figs. 9 and 10 for significantly thicker FG plate (i.e., the plate with L/h=10). It is clearly seen that in the case of thicker plates, as expected, the differences between the FSM results obtained from CLPT and FSDT theories have become more pronounced.

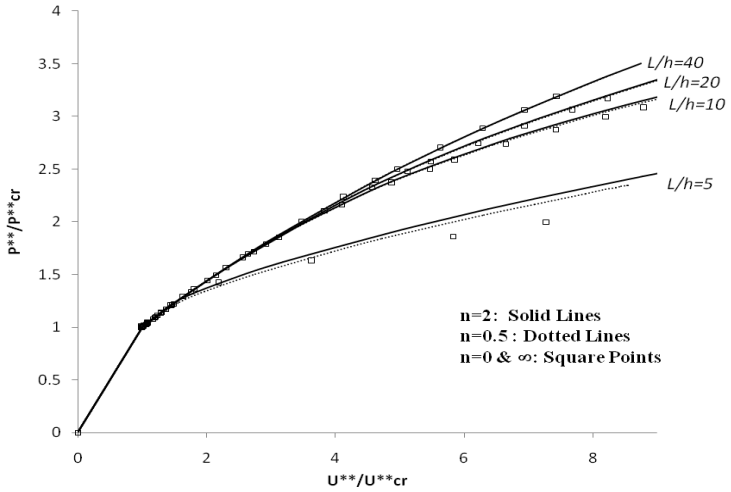

Fig. 11 Variation of non-dimensional total axial mean force ratio versus non-dimensional end-shortening ratio

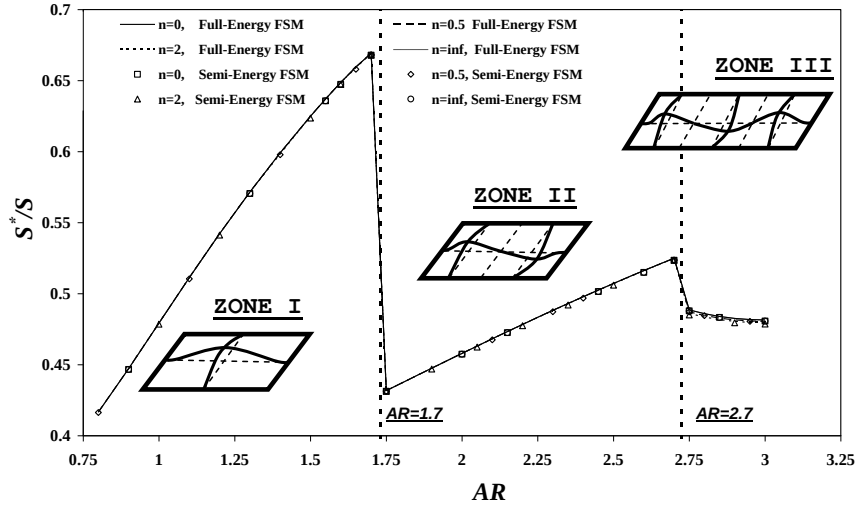

Fig. 12 Variation of initial post-buckling stiffness ratio via aspect ratio of thin FG plates

Finally, in order to study the effects of volume fraction index on post-buckling behavior of functionally graded plates, the variations of total axial mean force ratio (P^{**}/P_{cr}^{**}) versus non-dimensional end-shortening ratio (U^{**}/U_{cr}^{**}) are obtained and depicted in Fig. 11 for various length to thickness ratios (L/h=40, 20, 10 & 5) using FSDT FSM. It is clearly seen that for thin plates, the total axial mean force ratio (P^{**}/P_{cr}^{**}) is independent of volume fraction index and consequently the post-buckling response of FG plate (n=0.5 & 2) will be equal to those of pure plates (n=0 & ∞). However, it can be seen that the discrepancy between the results with various volume fraction index will be increased with increasing the thickness of plates.

7.3 Effects of aspect ratio on initial post-buckling stiffness ratio

The next step is to investigate the effects of aspect ratio on the post-buckling stable equilibrium path of FG plates just after buckling point. It is assumed that the width of plate is b=100 mm and thickness h is equal to 1 mm.

It is noted that the in-plane stiffness of plates will reduce as they encounter post-buckling behavior. Moreover, the initial post-buckling in-plane stiffness (S^*) and its ratio to pre-buckling stiffness (S) is an important factor (S^*/S) for design of plates encountering initial post-buckling behavior. The in-plane stiffness of plate is defined as the derivative of total mean force acting on plane (P) against end-shortening of plate (i.e., $\partial P/\partial \bar{u}$). The pre-buckling stiffness is a constant value as the plate demonstrates a linear behavior and can be calculated using buckling analysis based on Rayleigh-Ritz approach; however, as the post-buckling behavior of a plate is non-linear in nature, the post-buckling stiffness varies as the applied end-shortening progresses in post-buckling region. The initial post-buckling analyses are performed by incorporating full-energy CLPT FSM as well as semi-energy CLPT FSM for each aspect ratio. In this paper, (S^*) denotes the initial post-buckling stiffness just after the buckling point. Fig. 12 shows the variation of (S^*/S) against aspect ratio of FG plate. Moreover, the FG plates with different volume fraction indexes (i.e., $n=0, 0.5, 2, \infty$) are analyzed. Considering the results presented in Fig. 12, the following notes are remarkable.

For different values of FG material volume fraction index, the initial post-buckling stiffness ratio (i.e., S^*/S) is identical at each aspect ratio. It may lead to the hypothesis that the post-buckling stiffness ratio of thin FG plates might be independent of material properties (i.e., fraction of ceramic-metal components). Moreover, as the curves depicted in Fig. 12 are independent of base materials fraction index, they may be considered as a universal curve for a variety of material properties and may be used in sizing and preliminary design of thin FG plates encountering initial post-buckling behavior.

As far as a comparison between Fig. 4 and Fig. 12 is concerned, Fig. 4 demonstrates a garland shape for variation of buckling coefficient against aspect ratio of plate; however, Fig. 12 depicts a schematic *saw shape* curve for variation of initial post-buckling stiffness ratio against aspect ratio of a FG plate. It may be noted that the initial post-buckling stiffness ratio is quite sensitive to the buckling mode shape of rectangular FG plate. Therefore, the aspect ratio may be considered as a major factor for design of FG rectangular plates encountering initial post-buckling behavior.

8. Conclusions

A geometrically non-linear multi-term semi-energy finite strip, based on the concept of first order shear deformation theory, for the post-buckling analysis of geometrically thin and relatively thick FG plates is developed. In order to study the effects of through-the-thickness shearing stresses, the semi-energy FSM and the full-energy FSM based on the concept of classical laminated plate theory are also implemented. In order to check the validity and numerical performance of the developed methods, the finite element method is also applied. The study of the results has revealed that the semi-energy formulation has very good convergence properties and produces very accurate results by incorporating significantly less number of degrees of freedom than those required by the full-energy FSM and FEM. It is revealed that for the thin FG plates, the variations of non-dimensional load versus end-shortening is independent of ceramic-metal volume

fraction index. This means that the post-buckling response of thin FG plates are equal to those of pure isotropic plates. The garland curves corresponding to buckling behavior of mentioned FG plates are obtained using a Rayleigh-Ritz approach. Moreover, the variation of initial post-buckling behavior of thin FG plates with aspect ratio has been investigated. The analysis of results has revealed that initial post-buckling stiffness ratio of mentioned FG plates demonstrate a saw shape curve, which is independent of volume fraction index of base materials for FG plates. Moreover, the initial post-buckling stiffness ratio is highly influenced by the buckling mode shape of rectangular FG plates and by increasing the aspect ratio, a transition in buckle shape of plate will be occurred that leads to a drastic drop in initial post-buckling stiffness ratio. Finally, it may be concluded that when the design of thin FG rectangular plates for initial post-buckling behavior is concerned the aspect ratio of plate will play an important role in this behavior; however, the fraction of base materials may be negligible.

References

Allen, H.G. and Bulson, P.S. (1980), *Background to buckling*, McGraw-Hill, London.

Anandrao, K.S., Gupta, R.K., Ramchandran, P. and Venkateswara Rao, G. (2010), "Thermal post-buckling analysis of uniform slender functionally graded material beams", *Struct. Eng. Mech.*, **36**(5), 545-560.

Anandrao, K.S., Gupta, R.K., Ramchandran, P. and Venkateswara Rao, G. (2012), "Non-linear free vibrations and post-buckling analysis of shear flexible functionally graded beams", *Struct. Eng. Mech.*, **44**(3), 339-361.

Assaee, H. and Ovesy, H.R. (2007), "A multi-term semi-energy finite strip method for post-buckling analysis of composite plates", *Int. J. Numer. Meth. Eng.*, **70**(11), 1303-1323.

Assaee, H. and Ovesy, H.R. (2008), "Semi-energy finite strip post-buckling analysis of anti-symmetric cross-ply laminated plates concerning the effects of mechanical coupling", *Proceedings of the Fifth International Conference on Thin-Walled Structures*, Brisbane, Australia.

Assaee, H., Ovesy, H.R., Hajikazemi, M. and Sadr Lahidjani, M.H. (2010), "The Effects of Aspect Ratio on Post-buckling Behavior of Rectangular Plates of Functionally Graded Materials", *Proceedings of the Tenth International Conference on Computational Structures Technology*, Eds. B.H.V. Topping, J.M. Adam, F.J. Pallarés, R. Bru, M.L. Romero, Civil-Comp Press, Stirlingshire, UK.

Assaee, H., Hajikazemi, M. and Ovesy, H.R. (2012), "The effect of anisotropy on post-buckling behavior of laminated plates using semi energy finite strip method", *Compos. Struct.*, **94**(5),1880-1885.

Chai, G.B. (1989), "The effct of geometry and prescribed delaminations on the post-buckling behavior of laminated carbon-fiber reinforced plastic panels", PhD Thesis, University of Strathclyde.

Cheung, Y.K. (1976), *Finite strip method in structural analysis*, Pergamon Press, Oxford.

Cuong, B.H. (2013), "Buckling of thin-walled members analyzed by Mindlin-Reissner finite strip", *Struct. Eng. Mech.*, **48**(1), 77-91.

Dawe, D.J. (2002), "Use of the finite strip method in predicting the behavior of composite laminated structures", *Compos. Struct.*, **57**(1-4), 11-36.

GhannadPour, S.A.M and Alinia, M.M. (2006), "Large deflection behavior of functionally graded plates under pressure loads", *Compos. Struct.*, **75**(1-4), 67-71.

Hancock, G.J. (1981), "Nonlinear analysis of thin sections in compression", *J. Struct. Div., ASCE*, **107**(3), 455-471.

Kasaeian, S.H., Azhari, M., Heidarpour, A. and Hajiannia, A. (2011), "Inelastic local buckling of curved plates with or without thickness-tapered sections using finite strip method", *Int. J. Steel Struct.*, **12**(3), 427-442.

Kocaturk, T. and Akbas, S.D. (2012), "Post-buckling analysis of Timoshenko beams made of functionally graded material under thermal loading", *Struct. Eng. Mech.*, **41**(6), 775-789.

Koizumi, M. (1997), "FGM activities in Japan", *Compos. Part B Eng.*, **28**(1), 1-4.
Leissa, A.W. (1986), "Conditions for laminated plates to remain flat under inplane loading", *Compo. Struct.*, **6**(4), 261-270.
Markworth, A.J., Ramesh, K.S. and Parks, J.R. (1995), "Modeling studies applied to functionally graded materials", *J. Mater. Sci.*, **30**(9), 2183-2193.
Marguerre, K. (1937), "The Apparent Width of Plates in Compression", NACA-TM-833.
Ovesy, H.R., Loughlan, J. and GhannadPour, S.A.M. (2006), "Geometric non-linear analysis of channel sections under end shortening, using different versions of the finite strip method", *Comput. Struct.*, **84**(13-14), 855-872.
Ovesy, H.R. and Ghannadpour, S.A.M. (2007), "Large deflection finite strip analysis of functionally graded plates under pressure loads", *Int. J. Struct. Stab. Dyn.*, **7**(2), 193-211.
Ovesy, H.R. and Assaee, H. (2009), "Semi-energy finite strip post-buckling analysis of laminated plates concerning the effects of mechanical coupling", *Compos. Struct.*, **89**(1), 120-125.
Ovesy, H.R., Assaee, H. and Hajikazemi, M. (2009), "An investigation on post-buckling behavior of functionally graded plate using a semi energy finite strip approach", *Proceeding of the IJSSD Symposium on Progress in Structural Stability and Dynamics*, Hong Kong.
Ovesy, H.R. and Ghannadpour, S.A.M. (2009), "An exact finite strip for the calculation of relative post-buckling stiffness of isotropic plates", *Struct. Eng. Mech.*, **31**(2), 181-210.
Ovesy, H.R., Assaee, H. and Hajikazemi, M. (2011), "Post-buckling of thick symmetric laminated plates under end-shortening and normal pressure using semi-energy finite strip method", *Comput. Struct.*, **89**(9-10), 724-732.
Ovesy, H.R., Hajikazemi, M. and Assaee, H. (2012), "A novel semi energy finite strip method for post-buckling analysis of relatively thick anti-symmetric laminated plates", *Adv. Eng. Soft.*, **48**, 32-39.
Pham, C.H. and Hancock, G.J. (2013), "Shear buckling of channels using the semi-analytical and spline finite strip methods", *J. Construct. Steel Res.*, **90**, 42-48.
Praveen, G.N. and Reddy, J.N. (1998), "Nonlinear transient thermoelastic analysis of functionally graded ceramic-metal plates", *Int. J. Solid. Struct.*, **35**(33), 4457-4476.
Reddy, J.N. (2000), "Analysis of functionally graded plates", *Int. J. Numer. Meth. Eng.*, **47**,(1-3), 663-684.
Rhodes, J. and Harvey. J.M. (1977), "Examination of plate post-buckling behaviour", *J. Eng. Mech. Div., ASCE*, **103**(3), 461-478.
Sadr, M.H., Hajikazemi, M. and Ramezani-Oliaee, M. (2011), "Large deflection behavior of relatively thick functionally graded plates under pressure loads using higher order shear deformation theory", *Key Eng. Mater.*, **471-472**, 709-714.
Shen, S.H. (2009), *Functionally graded materials: nonlinear analysis of plates and shells*, CRC Press, Taylor & Francis Group.
Sherafat. M.H., Ghannadpour, S.A.M. and Ovesy, H.R. (2013), "Pressure loading, end- shortening and through- thickness shearing effects on geometrically nonlinear response of composite laminated plates using higher order finite strip method", *Struct. Eng. Mech.*, **45**(5), 677-691.
Sridharan, S. and Graves-Smith, T.R. (1981), "Post-buckling analysis with finite strips", *J. Eng. Mech. Div., ASCE*, **107**(5), 869-888.
Suresh, S. and Mortensen, A. (1998), *Fundamentals of functionally graded materials*, Maney, London.
Von-Karman, Th. (1910), *Encyklopadie der mathematischen wissenschaften*, IV4, Springer, Berlin.
Woo, J. and Meguid, S.A. (2001), "Nonlinear analysis of functionally graded plates and shallow shells", *Int. J. Solid. Struct.*, **38**(42-43), 7409-7421.
Yang, J. and Shen, S.H. (2003), "Non-linear analysis of functionally graded plates under transverse and in-plane loads", *Int. J. Nonlin. Mech.*, **38**(4), 467-482.